frontiers | Frontiers in Communications and Networks

TYPE Brief Research Report
PUBLISHED 02 July 2025
DOI 10.3389/frcmn.2025.1587497

OPEN ACCESS

EDITED BY
Jules M. Moualeu,
University of the Witwatersrand, South Africa

REVIEWED BY
Seong Ki Yoo,
Coventry University, United Kingdom
Ahmad Bazzi,
New York University Abu Dhabi, United Arab Emirates

*CORRESPONDENCE
Almir Maric,
almir.maric@etf.unsa.ba

RECEIVED 04 March 2025
ACCEPTED 30 April 2025
PUBLISHED 02 July 2025

CITATION
Maric A and Njemcevic P (2025) On the simulation and correlation properties of TWDP fading process.
Front. Commun. Netw. 6:1587497.
doi: 10.3389/frcmn.2025.1587497

On the simulation and correlation properties of TWDP fading process

Almir Maric* and Pamela Njemcevic

Department of Telecommunications, Faculty of Electrical Engineering, University of Sarajevo, Sarajevo, Bosnia and Herzegovina

This paper introduces a novel statistical simulator designed to model propagation in two-way diffuse power (TWDP) fading channels. The simulator employs two zero-mean stochastic sinusoids to simulate specular components, while a sum of sinusoids is used to model the diffuse one. Using the developed simulator, the autocorrelation and cross-correlation functions of the quadrature components, as well as the autocorrelation of the complex and squared envelope, are derived for the first time in literature for channels experiencing TWDP fading. The statistical properties of the proposed simulator are thoroughly validated through extensive simulations, which closely align with the theoretical results.

KEYWORDS

TWDP fading, sum-of-sinusoids (SOS), channel simulation, level crossing rate (LCR), wireless channel

1 Introduction

Mobile radio channel simulators are widely used as cost-effective alternatives to field trials, providing reproducible solutions for rapid performance evaluation by accurately replicating the statistical properties of real-world communication channels Xiao et al. (2006). Consequently, numerous small-scale fading simulators have been proposed to date for modeling various channel conditions, typically relying on filtering or sum-of-sinusoids (SoS) approaches, which are designed to capture both the first- and second-order statistics of signals following specific characteristics.

Among these, the earliest SoS simulators were designed for frequency non-selective Rayleigh channels Jakes and Cox (1994); Pop and Beaulieu (2001); Zheng and Xiao (2002); Xiao et al. (2006); Alimohammad et al. (2009); Wang et al. (2012). They are commonly used to model non-line-of-sight (NLOS) propagation conditions, where no strong specular components exist between the transmitter and the receiver. As a result, such signals consist solely of a diffuse component composed of many low-power scattered waves. Consequentially, corresponding small-scale fading simulators are created by representing the received signal as a superposition of a finite number of sinusoids, mostly with random amplitudes, frequencies, and/or phases. Thereby, to capture the statistical properties of signals received under the described conditions, Clark introduced a mathematical model assuming that the receiver receives $N \to \infty$ scattered waves with equal amplitudes, but with random angles of arrival (AoA) and random phases, mutually independent and uniformly distributed over $[-\pi, \pi)$ Clarke (1968). Clark's model has been validated through numerous measurements Skima et al. (2014) and has become a reference model for modeling propagation in NLOS conditions. As such, it has been used as the foundation of many Rayleigh SoS simulators, which, based on different assumptions about the behavior of sinusoidal phases and AoAs, aim to reproduce statistical properties of

the Clark's model, simultaneously maximizing computational efficiency by minimizing the number of employed sinusoids Skima et al. (2014).

The simulators mentioned above are also employed to model low-power scattered waves within Rician simulators, which are designed to simulate channels where the received signal consists of one strong specular component (typically line-of-sight, LoS) alongside a diffuse component. As a result, many Rician SoS simulators have been proposed to date, each exhibiting more or less desired statistical properties and specific computational efficiencies Xiao et al. (2006); Alimohammad et al. (2009); Wang et al. (2012).

However, to date, little attention has been given to the development of small-scale fading simulators that account for more than one dominant specular component, such as those required for two-wave with diffuse power (TWDP) fading channels. In these channels, the received signal contains two strong specular components in addition to numerous low-power scattered waves, which can lead to unique propagation characteristics including a bimodal distributed envelope (Maric et al., 2021; Figure 4) and phase (Maric and Njemcevic, 2025; Figure 4) characteristics and, under the certain conditions, performance worse than those observed in Rayleigh channels (Maric et al., 2021; Figure 5), which cannot be modeled using the existing simulators.

These, propagation conditions have been empirically validated in a variety of emerging wireless communication scenarios. For instance, TWDP fading has been observed in mmWave 5G networks utilizing directional antennas or antenna arrays Rappaport et al. (2015), as well as in wireless sensor networks operating in cavity environments Frolik (2007). Furthermore, ray-tracing simulations have confirmed the suitability of the TWDP model for characterizing outdoor mmWave propagation in train-to-infrastructure Zöchmann et al. (2019a) and vehicle-to-vehicle Zöchmann et al. (2019b) communication scenarios, particularly at 60 GHz in urban environments. Indoor mmWave measurement campaigns Zöchmann et al. (2019) have also demonstrated that the TWDP model accurately captures indoor propagation behavior. Additionally, TWDP fading has been shown to provide the best fit for near-body mmWave communication channels, both in the front and back body regions Mavridis et al. (2015). Moreover, similar fading conditions have been reported in static sensor networks placed within cavity environments, including buses, aircrafts Frolik (2007), and even inside large transport helicopters Frolik (2008). Accordingly, it is desirable to create a flexible and accurate channel simulator that can be effectively used for performance evaluation and validation of analytical expressions, derived for various designs of digital communication systems operating over the channels with TWDP fading.

Consequently, in this paper, the SoS-based simulator for modeling propagation in TWDP channels is proposed, being primary focused on generating correlated signal samples of TWDP multipath fading process. In the proposed simulator, the specular components are modeled as zero-mean stochastic sinusoids with pre-determined angles of arrival and random initial phases, while the diffuse component is simulated using the NLOS model proposed in Xiao et al. (2006). The simulator is used to derive the autocorrelation and cross-correlation functions of the quadrature components, as well as the autocorrelation of the complex envelope and its square, for signals propagating in TWDP channels. The statistical properties of the proposed simulator are compared with those calculated for the reference model, demonstrating excellent agreement between them.

Accordingly, we developed a SoS simulator capable of generating realistic TWDP fading waveforms, enabling the accurate evaluation of second-order statistics such as the level crossing rate (LCR) and average fade duration (AFD), which can be utilized for the design and optimization of channel coding schemes, interleaving strategies, and diversity techniques in channels exhibiting TWDP fading.

2 The reference TWDP channel model

TWDP model assumes that the normalized envelope of the received signal consists of two specular and diffuse components, so the normalized TWDP signal can be expressed as Durgin et al. (2002):

$$z(t) = \frac{1}{\sqrt{\Omega}}\left(V_1 e^{j\phi_1(t)} + V_2 e^{j\phi_2(t)} + n(t)\right) \tag{1}$$

where V_1 and V_2 are magnitudes of the specular components which remain constant over the local stationary interval, $\phi_1(t)$ and $\phi_2(t)$ are assumed to be independent and identically distributed (i.i.d.) uniform random variables, $n(t)$ is the zero-mean Gaussian-distributed diffuse component with an average power equals to $2\sigma^2$ and $\Omega = V_1^2 + V_2^2 + 2\sigma^2$ is the average power of the overall TWDP fading process.

In order to simulate the above defined TWDP fading process, let's assume communication scenario in which the receiver moves with constant velocity vector $\vec{v}$ (as illustrated in Figure 1) and in which the signal propagates from the transmitter to the receiver via two single-bounce specular reflections, as well as diffuse reflections from local scatterers in the vicinity of the receiver.

Due to the motion of the receiver, the instantaneous phase of each specular component's phase, $\phi_i(t)$ for $i = \overline{1,2}$, changes in time as:

$$\phi_i(t) = 2\pi\frac{l_i(t)}{\lambda} = \frac{2\pi}{\lambda}\sqrt{l_i^2 - 2l_i vt\cos\alpha_i(t) + (vt)^2} \tag{2}$$

where the angle of arrival $\alpha_i(t)$ can be considered as time invariant only during the local stationarity interval, i.e., $\alpha_i(t) \approx \alpha_i$. Within this interval, the instantaneous phase of each specular component, for $vt \ll l_i$, can be approximated as (Wolfram Research, 2025; 01.01.06.0001.01):

$$\begin{aligned}\phi_i(t) &\approx 2\pi\frac{l_i}{\lambda} - 2\pi\frac{vt}{\lambda}\cos\alpha_i + \mathcal{O}\left(\left(\frac{vt}{l_i}\right)^2\right)\\ &\approx \phi_i - 2\pi f_D t\cos\alpha_i\\ &\approx \phi_i + \dot{\phi}_i t\end{aligned} \tag{3}$$

where λ is the signal's wavelength, $f_D = v/\lambda$ is maximum Doppler frequency, $\dot{\phi}_i = -2\pi f_D\cos\alpha_i$ is the velocity of phase change as in (Golsmith, 2005; Equation 2.3), and l_i is propagation path length. Thus, the normalized baseband fading process of the received signal can be described as:

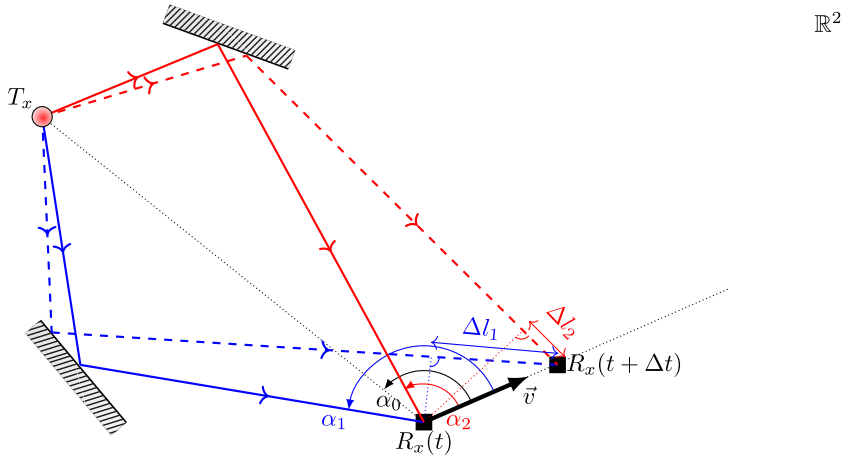

FIGURE 1
Channel model - illustration of specular reflections.

$$z(t) = \frac{1}{\sqrt{\Omega}}\left(V_1 e^{j(\phi_1+\dot{\phi}_1 t)} + V_2 e^{j(\phi_2+\dot{\phi}_2 t)} + n(t)\right) \tag{4}$$

where the uniformity of the specular components' phases $\phi_i(t)$ can be achieved by adopting uniform distribution of ϕ_i, regardless the chosen α_i. Under these conditions, the specular components can be modeled as zero-mean stochastic sinusoids with predetermined angles of arrival and random initial phases, which accurately capture their physical characteristics Xiao et al. (2006).

Considering the aforementioned and the fact that the specular and scattered components are all zero-mean with mutually independent initial phases, the autocorrelation of the TWDP complex envelope's in-phase component, $x(t) = \mathrm{Re}\{z(t)\}$, can be obtained by ensemble averaging, as:

$$\begin{aligned} R_{xx}(t, t+\tau) &= \mathbb{E}\{x(t)x(t+\tau)\} \\ &= \frac{V_1^2}{2\Omega}\cos\left(\dot{\phi}_1\tau\right) + \frac{V_2^2}{2\Omega}\cos\left(\dot{\phi}_2\tau\right) + \frac{1}{\Omega}\mathbb{E}\{n_x(t)n_x(t+\tau)\} \end{aligned} \tag{5}$$

where $\mathbb{E}\{\cdot\}$ is the statistical expectation operator, τ is the time lag and $\mathbb{E}\{n_x(t)n_x(t+\tau)\}$ is the autocorrelation function of the scattered waves' in-phase component, whose value depends on a chosen NLOS model. The autocorrelation of the quadrature component $R_{yy}(t, t+\tau)$, cross-correlations of the in-phase and quadrature components $R_{xy}(t, t+\tau)$ and $R_{yx}(t, t+\tau)$, and the autocorrelation of the complex envelope $R_{zz}(t, t+\tau)$, can be obtained in a similar manner, and here, the general expressions are not presented for brevity. Finally, the autocorrelation of the squared envelope, can be expressed as Equation 6;

$$\begin{aligned} R_{|z|^2|z|^2}(t, t+\tau) &= \mathbb{E}\{|z(t)|^2|z(t+\tau)|^2\} \\ &= \frac{1}{\Omega^2}\left[\mathbb{E}\{n_x^2(t)n_x^2(t+\tau)\} + \mathbb{E}\{n_y^2(t)n_y^2(t+\tau)\}\right. \\ &\quad + \mathbb{E}\{n_x^2(t)n_y^2(t+\tau)\} + \mathbb{E}\{n_y^2(t)n_x^2(t+\tau)\} \\ &\quad + \left(\mathbb{E}\{n_x^2(t)\} + \mathbb{E}\{n_y^2(t)\} + \mathbb{E}\{n_x^2(t+\tau)\}\right. \\ &\quad \left.\left. + \mathbb{E}\{n_y^2(t+\tau)\}\right)\left(V_1^2 + V_2^2\right) + \left(V_1^2 + V_2^2\right)^2 \right. \\ &\quad + 2\left(\mathbb{E}\{n_x(t)n_x(t+\tau)\} + \mathbb{E}\{n_y(t)n_y(t+\tau)\}\right) \\ &\quad \times \left(V_1^2\cos\left(\dot{\phi}_1\tau\right) + V_2^2\cos\left(\dot{\phi}_2\tau\right)\right) \\ &\quad + 2\left(V_1^2\sin\left(\dot{\phi}_1\tau\right) + V_2^2\sin\left(\dot{\phi}_2\tau\right)\right) \\ &\quad \times \left(\mathbb{E}\{n_x(t)n_y(t+\tau)\} - \mathbb{E}\{n_y(t)n_x(t+\tau)\}\right) \\ &\quad \left. + 2V_1^2V_2^2\cos\left(\left(\dot{\phi}_1 - \dot{\phi}_2\right)\tau\right)\right] \end{aligned} \tag{6}$$

where $\mathbb{E}\{n_y(t)n_y(t+\tau)\}$ is the autocorrelation of the scattered waves' quadrature component, $\mathbb{E}\{n_x(t)n_y(t+\tau)\}$ and $\mathbb{E}\{n_y(t)n_x(t+\tau)\}$ are their cross-correlations, while $\mathbb{E}\{n_x^2(t)n_x^2(t+\tau)\} + \mathbb{E}\{n_y^2(t)n_y^2(t+\tau)\} + \mathbb{E}\{n_x^2(t)n_y^2(t+\tau)\} + \mathbb{E}\{n_y^2(t)n_x^2(t+\tau)\}$ is the autocorrelation of the scattered waves' squared envelope, all dependent on underlying model chosen to simulate the behavior of the scattered waves.Within the isotropic scattering environment and under the narrow-band flat fading assumption, the diffuse component $n(t)$ can be mathematically modeled using Clark's model, as a superposition of N sinusoids. As such, it can be expressed as Xiao et al. (2006):

$$n(t) = \sqrt{\frac{2\sigma^2}{N}}\sum_{i=1}^{N} e^{j\left(2\pi f_D t\cos\beta_i + \varphi_i\right)} \tag{7}$$

where N is the number of scattered propagation paths, while β_i and φ_i are the angle of arrival and the initial phase of i-th path, respectively, assumed to be mutually independent and uniformly distributed over $[-\pi, \pi)$ for all i Clarke (1968).

So, in case when ideal Clark's model is used to model diffuse component, when $N \to \infty$, the reference expression for autocorrelation of the TWDP complex envelope's in-phase component can be obtained by inserting (Pätzold and Laue, 1998; Equation 2b) into Equation 5, as:

$$R_{xx}(\tau) = \frac{V_1^2}{2\Omega}\cos\left(\dot{\phi}_1\tau\right) + \frac{V_2^2}{2\Omega}\cos\left(\dot{\phi}_2\tau\right) + \frac{2\sigma^2}{2\Omega}J_0\left(2\pi f_D\tau\right) \tag{8}$$

where $J_0(\cdot)$ is the zero-order Bessel function of the first kind. Under the same assumptions, the reference expressions for autocorrelation

of the quadrature component, the cross-correlations of the in-phase and quadrature components, as well as the autocorrelations of the complex envelope and its square, can be obtained in a similar manner, by appropriately normalizing results given by (Skima et al., 2014, Equations 4a–4f), as:

$$R_{yy}(\tau) = R_{xx}(\tau) \tag{9a}$$

$$R_{xy}(\tau) = -R_{yx}(\tau) = \frac{V_1^2}{2\Omega}\sin\left(\dot{\phi}_1\tau\right) + \frac{V_2^2}{2\Omega}\sin\left(\dot{\phi}_2\tau\right) \tag{9b}$$

$$R_{zz}(\tau) = \frac{V_1^2}{\Omega}e^{-j\dot{\phi}_1\tau} + \frac{V_2^2}{\Omega}e^{-j\dot{\phi}_2\tau} + \frac{2\sigma^2}{\Omega}J_0(2\pi f_D\tau) \tag{9c}$$

$$\begin{aligned} R_{|z|^2|z|^2}(\tau) = {} & \frac{2\sigma^2}{\Omega}J_0(2\pi f_D\tau)\left[\frac{2\sigma^2}{\Omega}J_0(2\pi f_D\tau) + 2\frac{V_1^2}{\Omega}\cos\left(\dot{\phi}_1\tau\right)\right. \\ & \left. +2\frac{V_2^2}{\Omega}\cos\left(\dot{\phi}_2\tau\right)\right] \\ & +1 + 2\frac{V_1^2V_2^2}{\Omega^2}\cos\left(\left(\dot{\phi}_1 - \dot{\phi}_2\right)\tau\right) \end{aligned} \tag{9d}$$

Note that the derived expressions represent the statistical correlation properties of non-realizable stochastic reference model for the TWDP channel (since they are derived for $N \to \infty$). Nevertheless, these results are crucial, as they serve as the benchmark for evaluating the performance of any proposed TWDP simulator Pätzold and Hogstad (2006), which should aim to reproduce these properties as accurately as possible Patel et al. (2005).

3 The TWDP channel simulator

Based on the described reference model, the TWDP channel simulator is constructed following previously derived assumptions about the characteristics of the specular components. However, to simulate diffuse component using finite number of sinusoids, a detailed literature overview is performed, reveling the existence of many different models Jakes and Cox (1994); Pop and Beaulieu (2001); Zheng and Xiao (2002); Xiao et al. (2006); Alimohammad et al. (2009); Wang et al. (2012), etc. Among these, the model proposed by (Xiao et al., 2006, Equations 6a-6c, 7) (where β_i in Equation 7 is defined as $\beta_i = (2\pi i + \vartheta_i)/N$ and ϑ_i and φ_i are statistically independent and uniformly distributed over $[-\pi, \pi)$) is chosen due to its favorable simulation time, simplicity and pretty accurate correlation statistics Patel et al. (2005). So, based on the assumption that the initial phases of the specular components are random and independent from the initial phases of the scattered waves, chosen model is used to obtain autocorrelation and cross-correlation functions of the simulated TWDP signal, as:

$$R_{xx}(\tau) = R_{yy}(\tau) = \frac{V_1^2}{2\Omega}\cos\left(\dot{\phi}_1\tau\right) + \frac{V_2^2}{2\Omega}\cos\left(\dot{\phi}_2\tau\right) + \frac{2\sigma^2}{2\Omega}J_0(2\pi f_D\tau) \tag{10a}$$

$$R_{xy}(\tau) = -R_{yx}(\tau) = \frac{V_1^2}{2\Omega}\sin\left(\dot{\phi}_1\tau\right) + \frac{V_2^2}{2\Omega}\sin\left(\dot{\phi}_2\tau\right) \tag{10b}$$

$$R_{zz}(\tau) = \frac{V_1^2}{\Omega}e^{-j\dot{\phi}_1\tau} + \frac{V_2^2}{\Omega}e^{-j\dot{\phi}_2\tau} + \frac{2\sigma^2}{\Omega}J_0(2\pi f_D\tau) \tag{10c}$$

$$\begin{aligned} R_{|z|^2|z|^2}(\tau) = {} & \frac{2\sigma^2}{\Omega}J_0(2\pi f_D\tau)\left[\frac{2\sigma^2}{\Omega}J_0(2\pi f_D\tau) + 2\frac{V_1^2}{\Omega}\cos\left(\dot{\phi}_1\tau\right)\right. \\ & \left. +2\frac{V_2^2}{\Omega}\cos\left(\dot{\phi}_2\tau\right)\right] \\ & +1 + 2\frac{V_1^2V_2^2}{\Omega^2}\cos\left(\left(\dot{\phi}_1 - \dot{\phi}_2\right)\tau\right) \\ & -\frac{4\sigma^4}{\Omega^2}f_c(2\pi f_D\tau, N) - \frac{4\sigma^4}{\Omega^2}f_s(2\pi f_D\tau, N) \end{aligned} \tag{10d}$$

where $f_c(x, N)$ and $f_s(x, N)$ are defined as Xiao et al. (2006):

$$f_c(x, N) = \sum_{n=1}^{N}\left(\frac{1}{2\pi}\int_{\frac{2\pi n-\pi}{N}}^{\frac{2\pi n+\pi}{N}}\cos(x\cos\gamma)\mathrm{d}\gamma\right)^2 \tag{11}$$

$$f_s(x, N) = \sum_{n=1}^{N}\left(\frac{1}{2\pi}\int_{\frac{2\pi n-\pi}{N}}^{\frac{2\pi n+\pi}{N}}\sin(x\cos\gamma)\mathrm{d}\gamma\right)^2 \tag{12}$$

Obviously, the autocorrelation and cross-correlation functions given by Equation 10a; Equation 10b; Equation 10c do not depend on the number of sinusoids N, and they exactly match the desired second-order statistics of the reference TWDP model, given by Equation 8; Equation 9a; Equation 9b; Equation 9c. However, the autocorrelation function of the squared envelope, given by Equation 10d, differs from that calculated for the reference model. Despite this, it asymptotically approaches the desired autocorrelation Equation 9d as the number of sinusoids approaches infinity, and good approximation can be obtained even for relatively small number of sinusoids (e.g., $N \geq 8$) for most combinations of V_1, V_2, and $2\sigma^2$ (see Section 4.1 for detailed explanation).

It is important to note that the proposed simulator exhibits several key characteristics. First and foremost, it is wide-sense stationary (WSS), as its mean value remains constant and its autocorrelation function depends solely on the time difference τ, i.e., $R_{zz}(t, t+\tau) = R_{zz}(\tau)$ Pätzold and Hogstad (2006). Furthermore, by analyzing the derived correlation functions (Equations 10a-d), it can be shown that the results obtained by using proposed simulator can be reduced to those presented in [Xiao et al. (2006), Equations 12a–12d], which were calculated using a Rician fading simulator, when $V_2 = 0$ (with $K = V_1^2/\sigma^2$ and $\Omega = V_1^2 + 2\sigma^2$).

In addition, the proposed simulation model can be directly applied to generate uncorrelated fading waveforms for scenarios involving frequency-selective TWDP fading channels, MIMO systems, and diversity combining techniques, since $z_k(t)$, obtained by combining Equation 1 and Equation 7:

$$\begin{aligned} z_k(t) = {} & \frac{V_{1,k}}{\sqrt{\Omega_k}}e^{j\phi_{1,k}(t)} + \frac{V_{2,k}}{\sqrt{\Omega_k}}e^{j\phi_{2,k}(t)} \\ & + \sqrt{\frac{2\sigma_k^2}{\Omega_k}}\frac{1}{\sqrt{N}}\sum_{n=1}^{N}e^{j\left(2\pi f_D t\cos\alpha_{n,k}+\varphi_{n,k}\right)} \end{aligned} \tag{13}$$

where $\phi_{i,k}$ and $\varphi_{n,k}$ are mutually independent and uniformly distributed on $[-\pi, \pi)$ for all i, n and k, retains all the statistical properties of $z(t)$ defined by Equation 1, and $z_k(t)$ and $z_l(t)$ and are uncorrelated for all $k \neq l$.

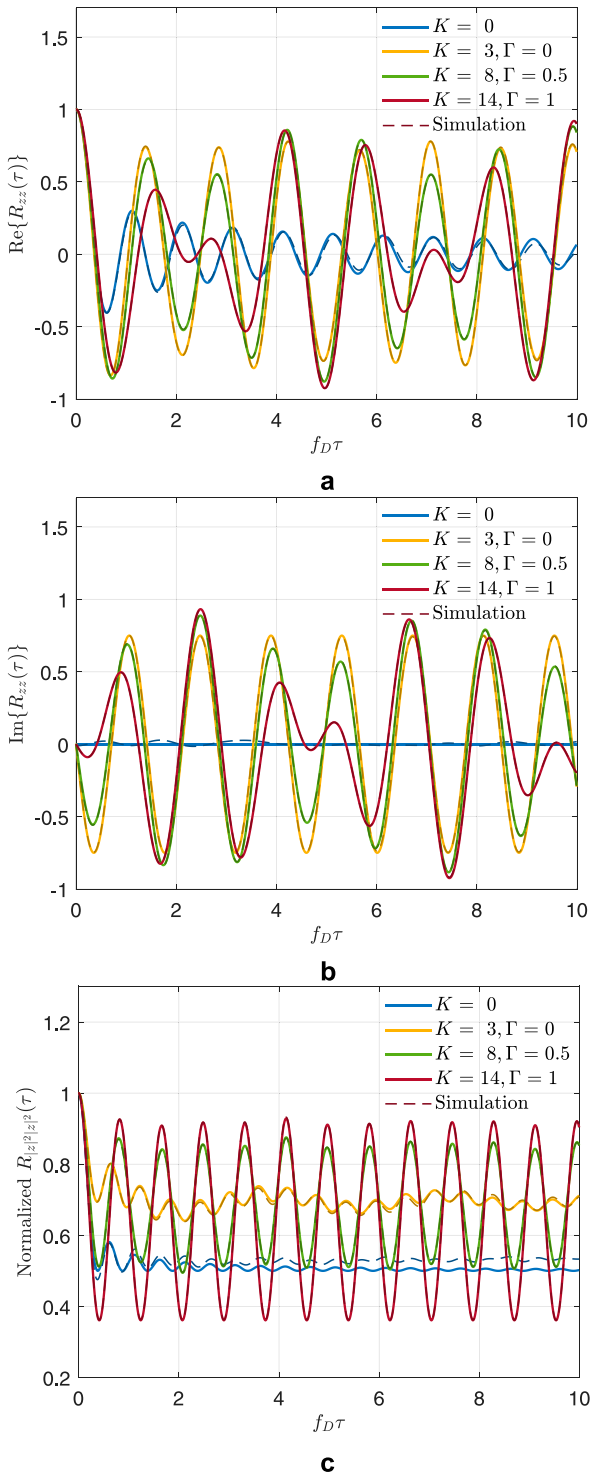

FIGURE 2
Correlation properties of TWDP complex envelope process. (α_1=π/4, α_2=2π/3). **(a)** The real part of the autocorrelation function of TWDP complex envelope. **(b)** The imaginary part of the autocorrelation function of TWDP complex envelope. **(c)** The autocorrelation function of TWDP squared envelope.

4 Numerical results

Verification of the proposed TWDP fading simulator is performed by comparing simulation results for finite N with those of the theoretical limits when N approaches infinity, for many different combinations of specular components' magnitudes V_1, V_2 and diffuse component's strength $2\sigma^2$. Thereby, in this section, instead of using specific values of V_1, V_2 and $2\sigma^2$, common TWDP parameters K and Γ, defined as: $K = (V_1^2 + V_2^2)/(2\sigma^2)$ and $\Gamma = V_2/V_1$, for $V_2 \leq V_1$, are used to describe specific propagation conditions in TWDP channels, in order to clearly perceive the impact of different fading severities on TWDP correlation characteristics.

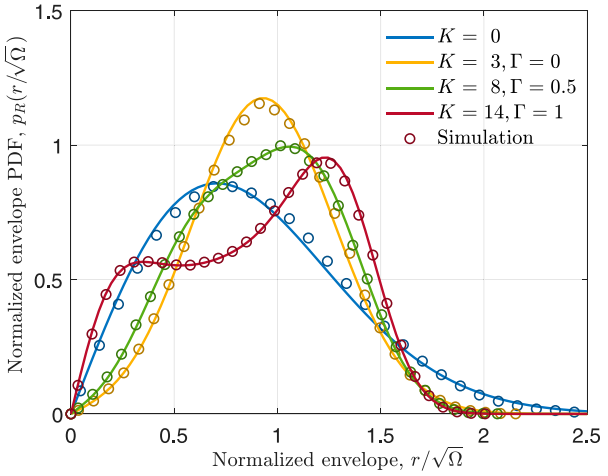

FIGURE 3
TWDP envelope PDF ($\alpha_1 = \pi/4$, $\alpha_2 = 2\pi/3$).

Accordingly, the simulations are conducted for many different combinations of TWDP fading parameters K and Γ, while $\Omega = 1$: $K = 0$ ($V_1 = V_2 = 0$), $K = 3$ and $\Gamma = 0$ ($V_1 = 0.866$, $V_2 = 0$ and $\sigma = 0.353$), $K = 8$ and $\Gamma = 0.5$ ($V_1 = 0.846$, $V_2 = 0.422$ and $\sigma = 0.236$), and $K = 14$ and $\Gamma = 1$ ($V_1 = 0.686$, $V_2 = 0.686$ and $\sigma = 0.183$) and different combinations of AoAs (α_1 and α_2). Throughout the simulations performed, the number of sinusoids is chosen to be $N = 8$ and all the ensemble averages for the simulation results are based on 500 random trials (as suggested in Xiao et al., 2006). Also, the normalized sampling period and maximum Doppler frequency are chosen to be $f_D T_s = 0.01$ (where T_s is the sampling period) and $f_D = 1000$ Hz, respectively.

4.1 Evaluation of correlation properties

Although extensive simulations are performed to evaluate TWDP correlation statistics, due to the space limitations, only simulation results obtained for the real and imaginary part of the autocorrelation of the complex envelope, together with the autocorrelation function of the envelope square, are shown in Figures 2a–c.

The corresponding statistics of the TWDP reference model given by Equations 9c, 9d are also included in the figures for comparison purpose, showing perfect match between simulated and theoretically obtained results in all cases except for the autocorrelation of the squared envelope in channel undergoing Rayleigh fading, as expected. Namely, in case when the strength of the diffuse component is large within the overall signal strength (i.e., when K is close to 0), the term $4\sigma^4[f_s(2\pi f_D\tau, N) + f_c(2\pi f_D\tau, N)]/(2\Omega^2)$ in Equation 10d becomes significant, producing notable difference between

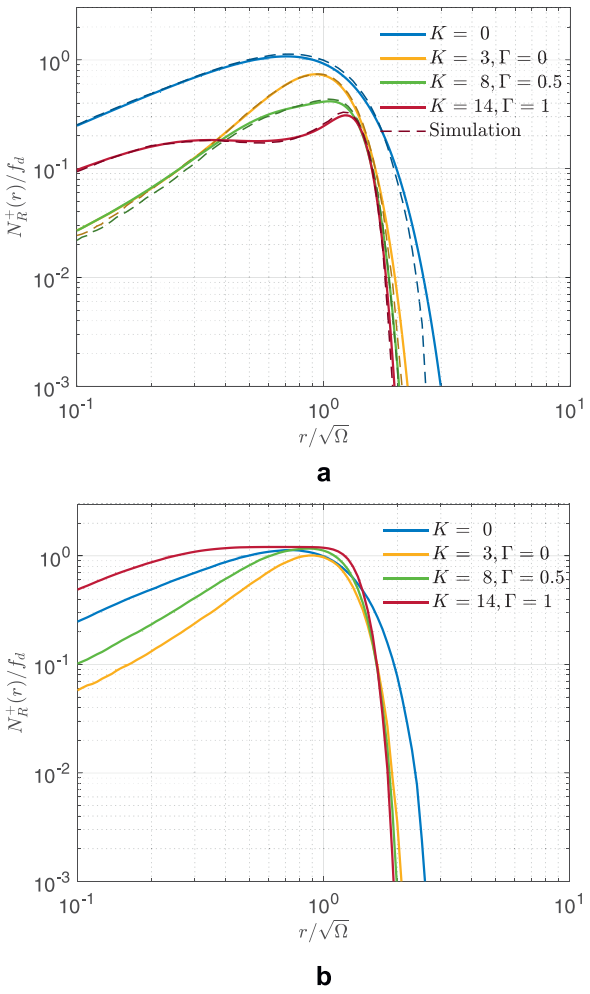

FIGURE 4
TWDP envelope LCR for different channel setups. **(a)** TWDP LCR (α_1=π/2, α_2=-π/2). **(b)** Simulated TWDP LCR (α_1=π/4, α_2=2π/3).

theoretical and simulated squared envelope autocorrelations. However, it is important to stress that the observed difference is the consequence of the model chosen to simulate diffuse component and can be reduced by using the one with more favorable characteristics. However, the scope of this paper was not to find the most accurate nor the most computationally efficient simulator. So underlying Rayleigh simulator is chosen from Xiao et al. (2006) mostly due to its simplicity and the fact that it has published results related to correlation functions obtained for Rician channels, which provide a reference point for verification of the results obtained using our simulator in case when TWDP fading collapses to Rician or Rayleigh. Accordingly, obtained results given in Figure 2 for Rayleigh and Rician fading are compared with those presented in (Xiao et al., 2006; Figures 3–5), showing a perfect match between all curves obtained for the same set of parameters.

4.2 Evaluation of envelope PDF

Figure 3 shows the fading envelope PDF obtained using the proposed TWDP simulator with the specified set of simulation parameters, along with the results from the analytical expression for the TWDP envelope PDF given in Maric et al. (2021). Although better agreement between the simulated and theoretical results can be achieved by increasing $N > 8$, the figure shows that the results obtained using proposed simulator agree very well with the theoretical ones, even for a small number of sinusoids ($N = 8$).

4.3 Evaluation of LCR

The simulation results of the normalized level crossing rate (LCR) for the proposed TWDP simulator are shown in Figures 4a,b. In Figure 4a, the results obtained using the proposed simulator are presented alongside those calculated using the analytical expression (Rao et al., 2014, Equation 36) derived for specific combination of AoAs in TWDP channels (i.e., when $\alpha_1 = 90^o$ and $\alpha_2 = -90^o$), showing excellent agreement in all considered cases. However, the expression (Rao et al., 2014, Equation 36) can only be used to obtain the LCR when both specular components arrive perpendicular to the direction of motion. For all other cases, no tools have been published to date for LCR evaluation. Therefore, the proposed simulator is the first tool that enables LCR evaluation for arbitrary TWDP parameters and AoAs.

For demonstration purpose, LCRs obtained using proposed simulator are plotted in Figure 4b, for different TWDP parameters and arbitrary AoAs, showing substantially different behaviors compared to the perpendicular cases presented in Figure 4a.

5 Conclusion

In this paper, the SoS-based TWDP channel simulator is proposed, enabling us to simulate Rayleigh, better-than-Rayleigh and worse-than-Rayleigh fading conditions. The simulator is constructed by using two zero-mean stochastic sinusoid with pre-selected Doppler frequencies and random initial phases, while the diffuse component is modeled using one of the existing Rayleigh channel simulators. For the described channel, analytical expressions for the autocorrelation and cross-correlation functions of quadrature components, as well as the autocorrelation of the complex envelope and its square, are first derived for the reference TWDP model. These expressions are then compared with those obtained using the proposed simulator for various combinations of channel and environmental parameters, demonstrating excellent agreement between them. Additionally, the proposed simulator is used to obtain diagrams of the envelope PDF and the LCR, which closely match those calculated using the existing analytical expressions. Since Rayleigh and Rician models are spatial cases of TWDP model itself, the results obtained using the proposed simulator (for specific sets of TWDP parameters) are finally compared to those from the literature obtained using the existing Rician/Rayleigh simulators, also showing the perfect match between them.

Accordingly, for the first time in the literature, a simulator is provided for accurate evaluation of first- and second-order statistics of signals propagating in channels with TWDP fading. As such, it can serve as a valuable tool for optimizing the design of interleaver/

deinterleaver and channel coding/decoding units in these channels, thereby contributing to the overall enhancement of wireless communication system performance in such environments.

Data availability statement

The original contributions presented in the study are included in the article/supplementary material, further inquiries can be directed to the corresponding author.

Author contributions

AM: Conceptualization, Formal Analysis, Software, Writing – original draft, Writing – review and editing. PN: Formal analysis, Software, Conceptualization, Writing – original draft, Writing – review and editing.

Funding

The author(s) declare that financial support was received for the research and/or publication of this article. This work was founded by Ministry of Science, Higher Education, and Youth of Canton Sarajevo, Bosnia and Herzegovina, under the grant 27-02-35-33087-23/24 (ASPK5GMM).

Conflict of interest

The authors declare that the research was conducted in the absence of any commercial or financial relationships that could be construed as a potential conflict of interest.

Generative AI statement

The author(s) declare that no Generative AI was used in the creation of this manuscript.

Publisher's note

All claims expressed in this article are solely those of the authors and do not necessarily represent those of their affiliated organizations, or those of the publisher, the editors and the reviewers. Any product that may be evaluated in this article, or claim that may be made by its manufacturer, is not guaranteed or endorsed by the publisher.

References

Alimohammad, A., Fard, S., Cockburn, B., and Schlegel, C. (2009). Compact Rayleigh and Rician fading simulator based on random walk processes. *Commun. IET* 3, 1333–1342. doi:10.1049/iet-com.2008.0297

Clarke, R. H. (1968). A statistical theory of mobile-radio reception. *Bell Syst. Tech. J.* 47, 957–1000. doi:10.1002/j.1538-7305.1968.tb00069.x

Wolfram Research (2025). Wolfram function site. Available online at: https://functions.wolfram.com.

Durgin, G., Rappaport, T., and de Wolf, D. (2002). New analytical models and probability density functions for fading in wireless communications. *IEEE Trans. Commun.* 50, 1005–1015. doi:10.1109/TCOMM.2002.1010620

Frolik, J. (2007). A case for considering hyper-Rayleigh fading channels. *IEEE Trans. Wirel. Commun.* 6, 1235–1239. doi:10.1109/twc.2007.348319

Frolik, J. (2008). On appropriate models for characterizing hyper-Rayleigh fading. *IEEE Trans. Wirel. Commun.* 7, 5202–5207. doi:10.1109/t-wc.2008.070968

Golsmith, A. (2005). *Wireless communications*. USA: Cambridge University Press.

Jakes, W. C., and Cox, D. C. (1994). *Microwave mobile communications*. Wiley-IEEE Press.

Maric, A., Kaljic, E., and Njemcevic, P. (2021). An alternative statistical characterization of TWDP fading model. *Sensors* 21, 7513. doi:10.3390/s21227513

Maric, A., and Njemcevic, P. (2025). On the conditional phase distribution of the TWDP multipath fading process. *arXiv*. doi:10.48550/arXiv.2502.03385

Mavridis, T., Petrillo, L., Sarrazin, J., Benlarbi-Delaï, A., and De Doncker, P. (2015). Near-body shadowing analysis at 60 GHz. *IEEE Trans. Antennas Propag.* 63, 4505–4511. doi:10.1109/tap.2015.2456984

Patel, C., Stuber, G., and Pratt, T. (2005). Comparative analysis of statistical models for the simulation of Rayleigh faded cellular channels. *IEEE Trans. Commun.* 53, 1017–1026. doi:10.1109/TCOMM.2005.849735

Pätzold, M., and Hogstad, B. (2006). Classes of sum-of-sinusoids Rayleigh fading channel simulators and their stationary and ergodic properties-Part I. *WSEAS Trans. Math.* 5, 222–230.

Pätzold, M., and Laue, F. (1998). Statistical properties of Jakes' fading channel simulator. VTC '98. 48th IEEE Vehicular Technology Conference 2, 712–718. doi:10.1109/VETEC.1998.683675

Pop, M., and Beaulieu, N. (2001). Limitations of sum-of-sinusoids fading channel simulators. *IEEE Trans. Commun.* 49, 699–708. doi:10.1109/26.917776

Rao, M., Lopez-Martinez, F. J., and Goldsmith, A. (2014). "Statistics and system performance metrics for the two wave with diffuse power fading model," in *2014 48th annual conference on information sciences and systems (CISS)*, 1–6. doi:10.1109/CISS.2014.6814106

Rappaport, T., Heath, R., Daniels, R., and Murdock, J. (2015). *Millimeter wave wireless communications*. Upper Saddle River, NJ, USA: Prentice Hall.

Skima, M. A., Ghariani, H., and Lahiani, M. (2014). A multi-criteria comparative analysis of different Rayleigh fading channel simulators. *AEU - Int. J. Electron. Commun.* 68, 550–560. doi:10.1016/j.aeue.2014.01.001

Wang, J., Ma, X., Teng, J., and Cui, Y. (2012). *Efficient and accurate simulator for Rayleigh and Rician fading*, Transactions of Tianjin University, 18, 243–247. doi:10.1007/s12209-012-1888-1

Xiao, C., Zheng, Y. R., and Beaulieu, N. C. (2006). Novel sum-of-sinusoids simulation models for Rayleigh and Rician fading channels. *IEEE Trans. Wirel. Commun.* 5, 3667–3679. doi:10.1109/TWC.2006.256990

Zheng, Y., and Xiao, C. (2002). Improved models for the generation of multiple uncorrelated Rayleigh fading waveforms. *IEEE Commun. Lett.* 6, 256–258. doi:10.1109/LCOMM.2002.1010873

Zöchmann, E., Blumenstein, J., Marsalek, R., Rupp, M., and Guan, K. (2019a). "Parsimonious channel models for millimeter wave railway communications," in 2019 IEEE Wireless Communications and Networking Conference (WCNC), 1–6. doi:10.1109/WCNC.2019.8885923

Zöchmann, E., Caban, S., Mecklenbräuker, C. F., Pratschner, S., Lerch, M., Schwarz, S., et al. (2019). Better than Rician: modelling millimetre wave channels as two-wave with diffuse power. *EURASIP J. Wirel. Commun. Netw.*, 2019. doi:10.1186/s13638-018-1336-6

Zöchmann, E., Hofer, M., Lerch, M., Pratschner, S., Bernadó, L., Blumenstein, J., et al. (2019b). Position-specific statistics of 60 GHz vehicular channels during overtaking. *IEEE Access* 7, 14216–14232. doi:10.1109/access.2019.2893136